2D Materials

RECEIVED
8 October 2016

REVISED
14 November 2016

ACCEPTED FOR PUBLICATION
28 November 2016

PUBLISHED
12 December 2016

LETTER

Effect of aging-induced disorder on the quantum transport properties of few-layer WTe_2

Wei Lai Liu[1,2,6], Mao Lin Chen[1,2,6], Xiao Xi Li[1,2], Sudipta Dubey[3], Ting Xiong[1,2], Zhi Ming Dai[1,2], Jun Yin[4], Wan Lin Guo[4], Jin Long Ma[5], Ya Ni Chen[5], Jun Tan[1,2], Da Li[1,2], Zhen Hua Wang[1,2], Wu Li[5], Vincent Bouchiat[3], Dong Ming Sun[1,2,7], Zheng Han[1,2,7] and Zhi Dong Zhang[1,2]

[1] Shenyang National Laboratory for Materials Science, Institute of Metal Research (IMR), Chinese Academy of Sciences (CAS), 72 Wenhua Road, Shenyang 110016, People's Republic of China
[2] School of Material Science and Engineering, University of Science and Technology of China, Anhui 230026, People's Republic of China
[3] University of Grenoble Alpes, CNRS, Institut Néel, F-38000 Grenoble, France
[4] State Key Laboratory of Mechanics and Control of Mechanical Structures, Key Laboratory for Intelligent Nano Materials and Devices of the Ministry of Education and Institute of Nanoscience, Nanjing University of Aeronautics and Astronautics, Nanjing 210016, People's Republic of China
[5] Institute for Advanced Study, Shenzhen University, Nanhai Avenue 3688, Shenzhen 518060, People's Republic of China
[6] These authors contributed equally to this work.
[7] Authors to whom any correspondence should be addressed.

E-mail: dmsun@imr.ac.cn **and** vitto.han@gmail.com

Keywords: WTe_2, quantum transport, disorder

Supplementary material for this article is available online

Abstract

The emerging physical phenomena found in transition metal dicalcogenides (TMDCs) have triggered vast investigations in recent years. Among them, nanoelectronics in WTe_2 devices have attracted particular attentions due to its exotic band structure that leads to exciting phenomena such as the predicted type-II Weyl semimetallic state. However, the thickness dependence of its quantum transport properties in the two-dimensional limit remains under debate. The major missing ingredient in the previous studies is the aging-induced disorder, as atomically thin layers of TMDCs are often known to be metastable in the ambient atmosphere. Here, we show systematic performance of low temperature quantum electronic transport of few-layer WTe_2. It is observed that aging-induced localized electronic states explains the low temperature Coulomb gap in transport measurements, leading to the anomalous magnetotransport which appears to be extrinsic. While few-layered WTe_2 shows clear metallic tendency in the fresh state, degraded devices first exhibited a re-entrant insulating behavior, and finally entered a fully insulating state. Correspondingly, a crossover from parabolic to linear magnetoresistance, and, upon further aging, leads to the observation of weak anti-localization. Our study reveals for the first time the correlation between the unusual magnetotransport and disorder in few-layered WTe_2, which is indispensable in providing guidance on its future device applications.

1. Introduction

The recent finding of known largest magnetoresistance in WTe_2 [1] triggered numerous studies in this layered material [2], including pressure-driven superconductivity [3] and the predicted new type of Weyl semimetal state [4–7]. Albeit a layered material, WTe_2 devices in the two-dimensional (2D) limit have been rarely reported, with its experimental investigations mostly restrained in the bulk regime (above 10 layers). Unlike other transition-metal dichalcogenides (TMDCs), instead of 2H phase, Td-phase of bulk WTe_2 occupies the lower energy state, whose two nearly perfectly compensated electron and hole bands result in a large unsaturated classical magnetotransport, with a parabolic dependence with the applied magnetic field B [8]. Meanwhile, strong anisotropy was found in its bulk form, which gives rise to some

exotic linear magnetoresistance in a specific measurement configuration [9]. Moreover, recent angle resolved photon electron spectroscopy studies showed subtleness of the band structure of bulk WTe_2 [10–13], intriguing possible peculiar electronic properties in the few layered scenario. In the 2D limit, electrostatic gate can, in principle, largely tune the carrier density, thus breaking down the electron-hole balance, leading to new opportunities.

Despite the fact that WTe_2 can be readily exfoliated thanks to the weak interlayer van-der-Waals bonding, ultra-thin WTe_2 is proven to rapidly age in ambient atmosphere like many of the TMDCs [14, 15]. Such air instability therefore hampers the further possibilities for nanoelectronic devices of, for example, few-layered WTe_2 field effect transistors [16]. Together with the extinction of optical contrast and Raman signal after air exposure [17], thin WTe_2 flakes were reported to exhibit anomalous quantum magneto-transport behaviors that strongly depend on thickness [18–20]. So far, a quantitative understanding of the correlation between quantum transport behavior and the imposed disorder has been missing not only on atomically thin WTe_2, but also on other two dimensional electronic systems. To address this matter, it is of great importance to assess the detailed transport properties including *IV* characteristics of few-layered WTe_2 devices in the parameter space of temperature and magnetic field.

In this letter, we show thinning of bulk WTe_2 down to a few layers via mechanically exfoliating high quality crystal. Atomically thin flakes of WTe_2 were systematically studied via Raman micro-spectroscopy and atomic force microscope (AFM) characterizations. We further fabricated the few-layered WTe_2 devices, and investigated their quantum electronic transport behavior with its evolution of aging. Strikingly, while the temperature dependence of few-layered WTe_2 showed clear metallic tendency in the fresh state, degraded devices first exhibited a re-entrant insulating behavior, and finally entered a fully insulating state. Correspondingly, a crossover from parabolic to linear magnetoresistance, and finally to weak anti-localization (WAL) is observed upon cooling. By investigating the current biased differential resistance of the few-layered WTe_2 devices, zero-bias dV/dI peaks were observed, indicating a Coulomb gap due to electron–electron interaction. Transmission electron microscopy (TEM) studies before and after air degradation of atomically thin WTe_2 further suggested that the material gradually forms amorphous islands, thus leading to localized electronic states. By studying the given sample upon aging, this work correlates the aging-induced structural disorders of a 2D material with the evolution of its quantum electronic transport properties.

2. Results and discussion

Single crystal WTe_2 was prepared via the Te self-flux method. Raw material powders with stoichiometric ratio of W (purity 99.9%):Te (purity 99.99%) = 1:49 were mixed and kept at 1000 °C for 8 h. The mixture was then cooled at the rate of 2 °C h^{-1}, followed by a centrifuge at 700 °C. Figure 1(a) shows the x-ray diffraction (XRD) pattern of powder (blue) and the exfoliated *a*–*b* plane (red) of the as-grown crystal shown in the inset. The highly oriented texture peaks of XRD reveal a single crystal of Td-WTe_2. We then applied the scotch tape method to exfoliate the bulk and deposited few-layered WTe_2 onto 285 nm thick silicon oxide grown on heavily doped silicon wafers. AFM images of such typical flakes with different number of layer are shown in figures 1 (b)–(d). In the reported studies, WTe_2 layer thickness varies between 0.6 and 1.2 nm [17, 18, 21–23]. Here, we evaluated the thickness of a monolayer WTe_2 to be 0.79 nm, upon a statistics of more than 20 measured flakes. Such thickness profiles are given in figures 1(e)–(g), cutting along the corresponding dashed lines in figures 1(b)–(d). We notice that the probability of having monolayer WTe_2 was rather low, we mostly had constant yields of above two layer WTe_2 thin flakes.

Raman studies of WTe_2 were performed, in order to comprehend its lattice dynamics and the effects caused by air-degradation. Thin layers are exfoliated in ambient atmosphere for AFM and Raman measurements. Figure 1(h) displays the Raman spectra of WTe_2 of 2–8 layers probed by a 532 nm wavelength laser. The bi-layer WTe_2 shows least peaks and lowest signal, with 6 distinct Raman bands observed around 86.7, 108.3, 120.0, 135.6, 164.2 and 215.3 cm^{-1}, respectively, in agreement of those reported in previous works [21–23]. All spectra are fitted via single Lorentzian and renormalized for visual clarity as seen in figure 1(h). It is worth noting that the peak at wave number of about 86 cm^{-1} splits into two bands above 4 layers, as highlighted in the dashed box in figure 1(h). This anomaly was not reported before and may provide a new reference for distinguishing the number of layers in thin WTe_2.

Since ultra-thin WTe_2 is known to degrade rapidly due to air instability [17], it is of importance to have quantitative evaluation of its lifetime in ambient conditions. Figure 1(i) shows a time evolution of a 4-layered flake under 532 nm laser with 0.7 mW power. Clear decay of the peaks intensity with increasing time can be seen. Time evolution of the 215 cm^{-1} peak is plotted in figure 1(j). It is seen that the intensity as a function of time follows an exponential decay, which is fitted to a lifetime of $\tau_{air} = 62$ min. On the opposite, thicker (more than 5 layers) flakes retain their Raman signal for days and even weeks, as they are screened by surface passivation of the top layer. It is noteworthy that, the strongly degraded (exposed in air for long time) WTe_2 thin layers lost most of its optical

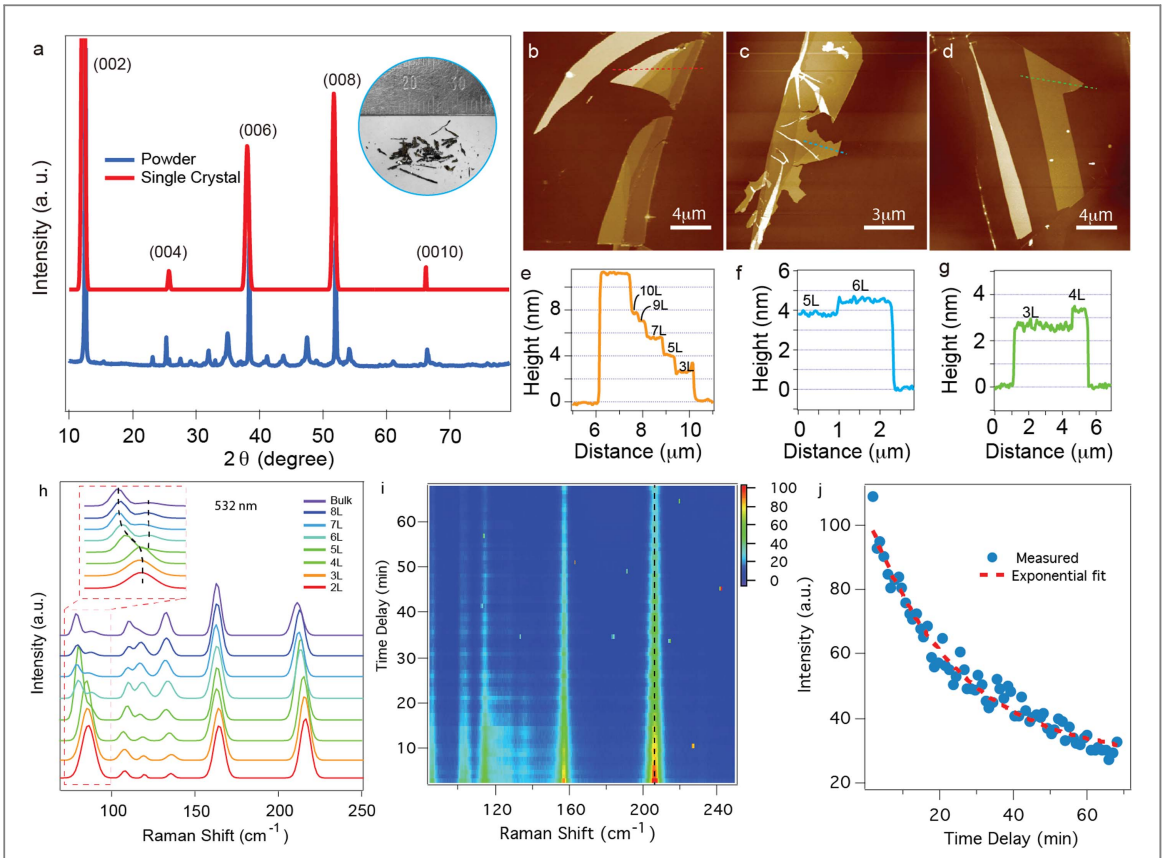

Figure 1. (a) XRD pattern of Td-WTe_2. Red and blue are patterns for single crystal and powder samples, respectively. Inset in a) shows an optical image of the as-grown mm-sized crystal. (b)–(d) AFM images of typical WTe_2 flakes with different thickness. Height profiles along corresponding dashed lines are given in (e)–(g). (h) Green laser with 532 nm Raman spectra for WTe_2 with different number of layers. Curves are fitted by single Lorentzian of each measurable peaks. Inset shows renormalized Raman characteristics at wavenumbers below 100 cm^{-1}. (i) Time evolution of Raman intensity for a four-layered WTe_2. (j) Peak intensity (highlighted by dashed line in (i) as a function of time delay. Red dashed line gives the exponential fit.

contrast, while AFM scans show almost the same height (figure S1). Energy dispersive spectrum (EDS) of the strongly disordered few-layered WTe_2 flake indicates the absence of oxygen (figure S2). Stoichiometry ratio of W and Te elements evaluated from EDS mapping, before and after heat treatment, are both fluctuating around 2 (figure S3 and table S1). Moreover, Raman peak widths (figure S4) are not evolving with time. The explanation for this can be that the amorphous clusters in the flake are Raman-inactive, while the crystalline parts are Raman-active and keep their partial contribution to the total Raman signal. As time evolves, the total signal intensity decreases because of the increasing amount of amorphous clusters, this together with AFM and EDS analysis, are in agreement with the process of amorphization as will be discussed by TEM observations in the following sections. As time evolves, the total signal intensity decreases because of the increasing amount of amorphous clusters, this together with AFM and EDS analysis, are agree with the process of becoming amorphous as will be discussed by TEM observations in the following sections. As the major possible detrimental factors in the atmosphere may be either oxygen or water, more controllable degrading experiments by exposing few layers of WTe_2 to O_2 or water vapour could be interesting for better understanding the mechanism of degradation in few layered WTe_2.

We now come to the fabrication of few-layered WTe_2 devices. Multiple samples of few-layered WTe_2 with different thickness were contacted by Ti(5 nm)/Au(60 nm) electrodes via standard e-beam lithography. As discussed in the previous section, ultra-thin WTe_2 flakes suffer from air instability. To minimize exposure to air and hence to measure in a 'fresh' state the devices, a resist (PMMA) layer was immediately (after a few minutes of exposure) spun on few layered WTe_2 flakes after exfoliation. Thin flake identification under optical microscope and aligned electrode lithography are then performed with the PMMA protection. Electrodes metallization was done followed by rapid re-spun of PMMA resist and a second exposure was made to open windows on the bonding pads, with the rest of PMMA resist kept throughout the measuring process (schematic in figure 2(a)). Figure 2(b) exhibits the field effect curves at T = 5 K of a 4-layered device on standard 280 nm thick SiO_2 with doped Si gate. It is seen that PMMA protected few-layered WTe_2 devices show rather low sheet resistance but also poor gate-tunability. For square sample, by using the capacitive coupling model, electron mobility μ satisfies the relation $\sigma = ne\mu$, where σ is the

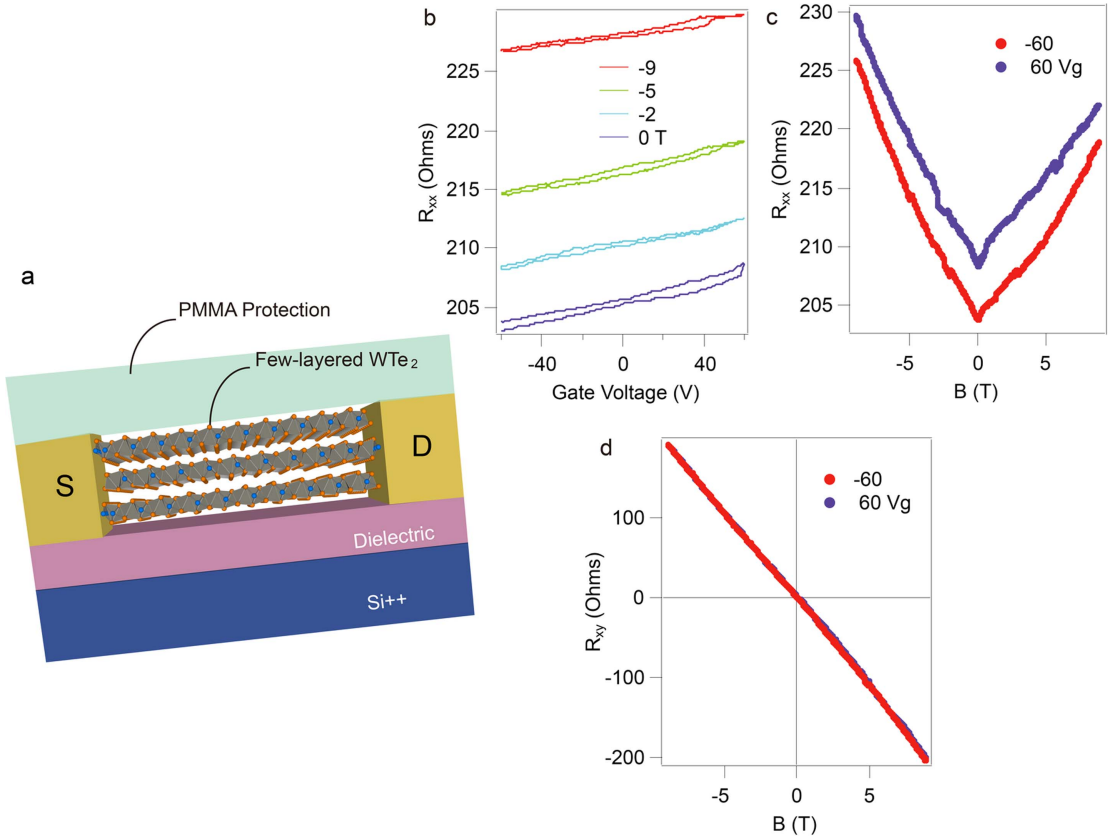

Figure 2. (a) Schematic picture of few-layered WTe_2 device protected by PMMA as described in the main text. (b) Field effect of the 4-layered device at different magnetic field. (c) Magnetoresistance measured at −60 and 60 V gate voltages, with their corresponding transverse resistance R_{xy} plotted in (d). Data were measured at 5 K.

conductivity, n the carrier density, e electron charge, and $ne = CV_g$, with C the capacitance of dielectric layer, V_g the gate voltage. Neglecting doping level dependence, it can be simplified to $\mu = (1/C)(\mathrm{d}\sigma/\mathrm{d}V_g)$. Mobility can therefore be evaluated from the slope of $\sigma - V_g$ plot. We thus estimate μ in the measured device to be around 74 $\mathrm{cm^2\,V^{-1}\,s^{-1}}$, much higher than reported elsewhere [18]. Moreover, while the field effect curves remain of similar shapes, they can be shifted by applied external magnetic field, as shown in figure 2(c). Meanwhile, the transverse resistance however is almost electric field-independent (figure 2(d)). We notice that a surface-doping non-local conductivity model was also proposed for relatively thick WTe_2 samples [24].

In the following, we will discuss the quantum electron transport properties of few-layered WTe_2. A standard 4-probe method was used, while the magnetic field was applied perpendicularly to the exfoliated a–b plane of WTe_2 crystal. To start with, figure S5(a) shows the temperature dependence of bulk resistance (RT curves) at different magnetic fields. As can be seen, bulk WTe_2 has its symbolic 'turn on' behavior, giving rise to the metal-to-insulator transition when subjected to magnetic field. Another perspective to present the curves is shown in figure S5(b), i.e., magnetoresistance at different temperatures. All curves show parabolic B-dependence of the magnetoresistance signal. Indeed, here the magnetoresistace (MR) can be explained by the classical two band model, written as [8]:

$$\frac{\Delta R}{R} = \frac{\mu_e\mu_h(n\mu_e + p\mu_h)(p\mu_e + n\mu_h)B^2 - (p-n)^2\mu_e^2\mu_h^2B^2}{(n\mu_e + p\mu_h)^2 + (p-n)^2\mu_e^2\mu_h^2B^2}, \quad (1)$$

where R is the resistance, n, p, μ_e and μ_h are electron and hole densities and mobilities, B is the magnetic field. In the case of fully balanced electron and holes, it reduces to a quadratic form $\frac{\Delta R}{R} = \mu_e\mu_hB^2$. Curves in figure S1(b) follow closely this quadratic trend, indicating the well-known electron-hole compensation in the bulk.

Figure 3(a) shows the 4-probe RT curves under different magnetic fields of a typical 4-layered WTe_2

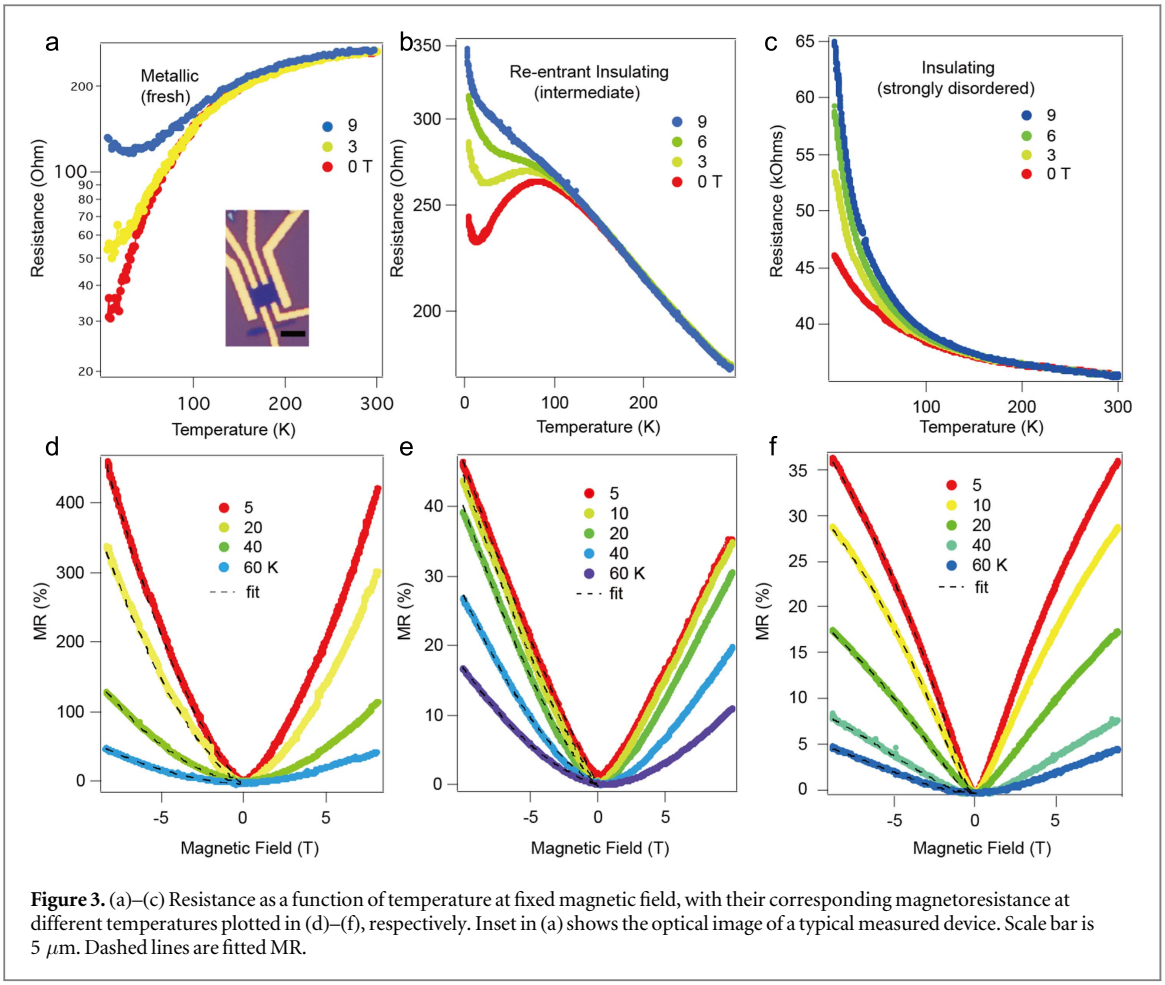

Figure 3. (a)–(c) Resistance as a function of temperature at fixed magnetic field, with their corresponding magnetoresistance at different temperatures plotted in (d)–(f), respectively. Inset in (a) shows the optical image of a typical measured device. Scale bar is 5 μm. Dashed lines are fitted MR.

device protected by PMMA. Thanks to the capping layer, the device showed clear metallic state, as opposed to the insulating behavior reported elsewhere [18]. Interestingly, magnetoresistance at different temperatures of the 4-layered device does not follow exactly the parabolic B-dependence, as shown in figure 3(d). Instead, an additional correction of linear magnetoresistance is needed to fit the data (dashed lines in figure 3(d)). Thus the fit is given by $\frac{\Delta R}{R} = \alpha B^2 + \beta B$, where α and β are fitting parameters.

To further investigate the influence of imposed disorder in few-layered WTe_2, we measured a 4-layer sample, which was exposed to air for 1 week without the protecting PMMA layer. Strikingly, the device with fairly disordered state showed a re-entrant insulating behavior (figure 3(b)), with a metallic intermediate region appearing in the temperature range of 10–80 K at zero magnetic field. The intermediate metallic state was then totally suppressed by cooling with a magnetic field above 6 T. The re-entrant insulating behavior has been already reported in other systems such as amorphous superconducting film [25], and ultra-thin manganite compounds [26], and was attributed to localization or electronic phase separation, respectively. In the present system, we speculate that the onset of metallic conduction of WTe_2 appears only in the intermediate temperature range, and electrons stay localized both at room temperature and at the lowest temperature region. Magnetoresistance of this device (exposed to air for a week without PMMA protection) is shown in figure 3(e), which gives much more pronounced characteristics of linear B-dependence compared to the fresh sample shown in figure 3(d). The increased disorder with concomitantly enhanced linear MR, and persisting quadratic B-dependence at low field, point towards a possible disorder-driven linear MR [27–29]. It is interesting to note that the disorder induced magneto-resistance change here (linear MR to WAL) is quite similar to another layered 2D telluride system, Bi_2Te_3, as reported previously [30, 31]. From the applied physics point of view, a linear non-saturating magnetoresistance is highly desired for the design of magnetic sensors. Few layered WTe_2 therefore seems to be one of the promising candidates.

As shown in figure 3(c), when the flakes are strongly degraded (either by long exposure to air or by heating to above 200 °C for a few min in air) WTe_2 devices with number of layers between 3 and 8 all show exponentially increasing resistance upon cooling, i.e., a complete insulating state. Figure 3(f) shows the magnetoresistance of the insulating 4-layered device at different temperatures, which drastically differs from the metallic and re-entrant insulating states. A WAL characteristic was observed, which is described by the Hikami–Larkin–Nagaoka theory [32]:

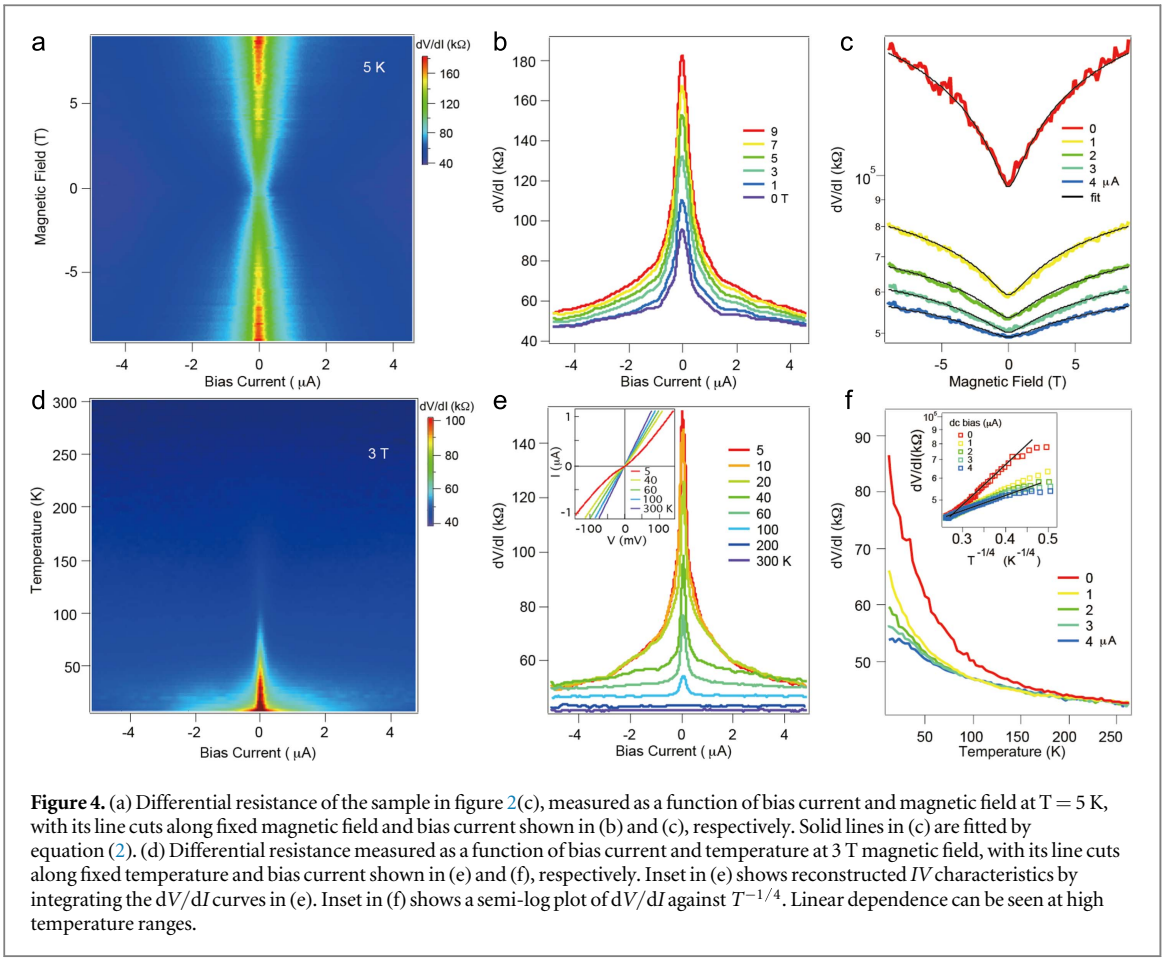

Figure 4. (a) Differential resistance of the sample in figure 2(c), measured as a function of bias current and magnetic field at T = 5 K, with its line cuts along fixed magnetic field and bias current shown in (b) and (c), respectively. Solid lines in (c) are fitted by equation (2). (d) Differential resistance measured as a function of bias current and temperature at 3 T magnetic field, with its line cuts along fixed temperature and bias current shown in (e) and (f), respectively. Inset in (e) shows reconstructed *IV* characteristics by integrating the dV/dI curves in (e). Inset in (f) shows a semi-log plot of dV/dI against $T^{-1/4}$. Linear dependence can be seen at high temperature ranges.

$$\Delta\sigma \propto \Psi\left(0.5 + \frac{B_\Phi}{|B|}\right) - \ln\left(\frac{B_\Phi}{|B|}\right), \qquad (2)$$

where Ψ is the digamma function, and $B_\Phi = \frac{\hbar}{4eD}\tau_\phi^{-1}$, with D the diffusion constant and τ_ϕ the electron phase coherent time. In equation (2), we neglected other spin–orbit coupling terms which play negligible role in the fitting process. WAL observed in 2D electronic systems, including topological insulators and graphene, are often explained by a π Berry phase captured by electrons through closed trajectory [33, 34]. Recent studies in 3D Dirac semimetal, 3D Weyl semimetal, as well as chemical vapor deposited TMDCs also showed WAL phenomenon at relatively low field range [35, 36].

In mesoscopic devices, differential resistance dV/dI as a function of bias current is a useful tool to analyze the transport behavior. Figure 4(a) shows a color map of dV/dI at T = 5 K in the dc bias current and magnetic field space for the same device measured in figures 3(c) and (f) (multiple strongly degraded samples with different number of layers all showed similar dV/dI behavior). Line cuts along fixed B show a strong zero-bias resistance peak, as shown in figure 4(b). This zero-bias anomaly is a characteristic of a Coulomb gap induced by the local electron charging effect. In a disordered system, electron transport occurs via variable range hopping, while Coulomb interactions between different hopping sites are dominating and lead to a low-bias barrier at low temperature. Line cuts along fixed bias current of figure 4(a) are also plotted, as shown in figure 4(c). It is seen that at low bias, the magnetoresistance shows highest absolute values, while all cases, including the zero-biased, it can be well fitted by the WAL using equation (2). The resulting B_{Phi} extracted for each bias current are plotted in figure S6(a). One can see that B_{Phi} increases from the low bias Coulomb blockade regime to the high bias regime where in principle the Coulomb gap is overcome by the bias energy. For comparison, B_{Phi} fitted from temperature dependence in figure 3(f) are plotted in figure S6(b), which shows a rather linear trend, consistent with reported elsewhere [18].

An important picture to evaluate the Coulomb gap in the studied WTe_2 few layers is the temperature dependence of the dV/dI versus bias current. Figure 4(d) shows a representative color map of such measurement under 3T magnetic field. It is clearly observed in the line cuts along fixed temperature (figure 4(e)) that the dV/dI curves above 200 K are completely flat, while the zero-bias anomaly starts to show up below 200 K, and increase with lowering the temperature as expected for a typical Coulomb gap anomaly. To further investigate the output characteristics, we plotted in *IV* curves by integration of differential resistance, shown in the inset of figure 4(e). One

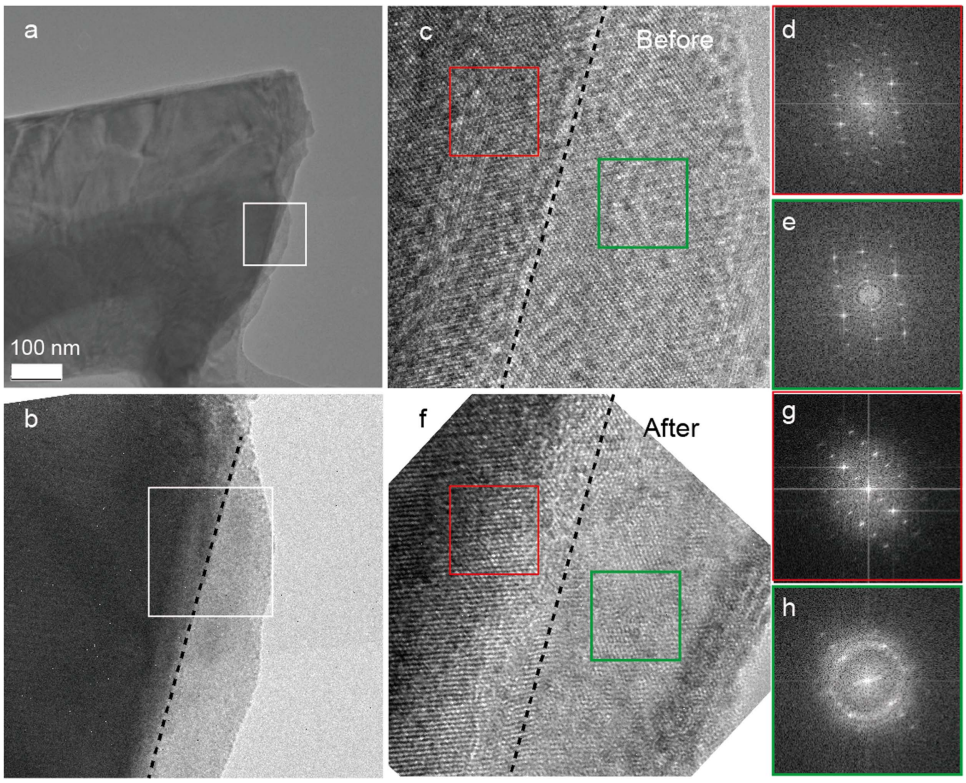

Figure 5. (a) TEM image of WTe_2 flake, whose white boxed area is shown in (b). Boxed area in (b) is then zoomed for high resolution TEM measurement. (c) and (f) are images taken before and after thermal degradation of the flake in air, respectively, with their boxed area performed FFT, as shown in (d)–(e) and (g)–(h). Dashed lines in (b)–(f) highlights the boundary between thick and thin WTe_2. Notice (f) is rotated to align with (b) and (c) for visual clarity.

can see that in the high temperature range, *IV* curves are linear, corresponding to Ohmic transport. At base temperature of 5 K, *IV* develops into a semiconductor-like nonlinear state. Finally, we examine *RT* curves at different bias current, as shown in figure 4(f), whose high temperature range can be well explained by the 3D Mott's hopping law $R \propto \exp[(T_0/T)^{1/4}]$ (inset of figure 4(f)), while divergence are found at low temperatures. One possibility to explain the Mott's hopping behavior is the extremely small electron scattering distance that is even smaller than the few-layer thickness, and the surface charging effect is the main cause of the observed Coulomb blockade phenomenon. Surprisingly, it is noticed that even for fresh metallic WTe_2 devices which were protected to minimize air exposure, the Coulomb gap already started to develop below 60 K, as shown in figure S7. Interestingly, recent study suggested such gap to be of a possible quantum spin Hall origin [37]. Our above analyses suggest that this nonlinear *IV* characteristic is mainly caused by disorder, as indicated by the correlated increase of Coulomb gap.

In order to reveal the microscopic origination of the observed unusual magnetotransport, we performed TEM analysis of few-layered WTe_2 before and after heat treatment. As shown in figures 5(a) and (b), an ultra-thin area of the freshly prepared specimen (see methods section) was located. High-resolution TEM image shown in figure 5(c) indicates good crystalline structure on both sides of the thick and thin areas separated by the black dashed line. Fast Fourier transform (FFT) of boxed areas in figures 5(d) and (e) shows almost identical lattice symmetry on both sides, which proves the pristine lattice in ultra-thin WTe_2 layers. By taking out the TEM specimen and heating in air at 200 °C for 5 min, the thin WTe_2 becomes significantly degraded. The same flake was re-located after the heat treatment, as given in figure 5(f). It can be seen that on the left side (thick region), lattice are preserved as its fresh state. However, on the right side of the dashed line (thin region), the lattice becomes much degraded as expected, and exhibits typical amorphous features, as further evidenced by its FFT in figure 5(h) presenting the ring-shape compared to the discrete spots shown in figures 5(g) and (d)–(e). By examining the thin part of WTe_2 in figure 5(f), it is found that WTe_2 crystalline clusters of about 10×10 atoms are embedded in the amorphous matrix when strongly degraded, agree with the hopping-like localized behavior in transport measurements.

Indeed, when plotted as differential conductance dI/dV against bias voltage, the Coulomb gap Δ in strongly degraded sample can be estimated to be of the order of few tens of meV at 5 K (figure S8(a)). The same plot measured in a 'metallic' sample as shown in figure S8(b) exhibits also such gap below 60 K, with however much lower magnitudes of a few tens of μeV.

The rather low mobility of about 74 cm^2 V^{-1} s^{-1} extracted in such 'metallic' WTe_2 field effect transistor may be already limited by the degradation. PMMA is known to provide an inert protection layer to avoid from contamination and/or air degradation. Nevertheless, it is also interesting to use hexagonal boron nitride (h-BN) as a capping layer to protect the ultra-thin samples from degradation as the neutrality and flatness provided by BN is unmatched. It is seen that even everything was done as fast as possible in the ambient atmosphere (figure S9), the ultra-thin WTe_2 flake protected by h-BN is already no longer in a metallic regime (figure S10). Large zero-bias dV/dI peak starts to develop below 150 K, shown in figure S10b. Clearly, the exposure-to-air time of 15 ~ 20 min is more than enough to destroy the 'fresh' state in few-layered WTe_2 flakes.

3. Conclusions

As a summary, in few layered WTe_2 devices, we found a transition from the metallic state to a re-entrant insulating state, and finally to full insulating state that is correlated with increasing disorder. Correspondingly, a crossover from semi-metallic to linear magnetoresistance and finally to WAL is observed. Systematic studies by Raman, AFM, TEM, and differential resistance measurements have provided for the first time microscopic understanding of air instability of ultra-thin WTe_2. It is thus expected that by reducing surface degradation, such as the recently developed boron nitride (h-BN) encapsulation technique [38, 39], the pristine quality of 2D WTe_2 may be preserved (figure S8) and may give rise to higher electron mobility, leading to WTe_2 transistors with better performances, as well as profound physics such as the seek for experimental proof of type-II Weyl fermions.

4. Methods

Raman and AFM measurements were carried out using a Renishaw and the Bruker Icon system, respectively. 532 nm wave length and 0.5 mW power were applied in this study. To limit the aging of ultra-thin WTe_2 devices, we spin coated a layer of PMMA resist immediately after exfoliation. Degraded samples are then studied without PMMA capping layer. We found that heating on a hot-plate above 200 °C gives similar results as long air exposure (i.e., by keeping the sample in air for a few weeks or even month). Measurements carried out in figure 2 were using excitation of 5 μA ac current from Stanford SR830 lock-in with a bias resistor. While data in figure 3 were acquired using a four probe dc bias configuration, added by an ac lock-in signal to obtain the dV/dI curves. Lock-in excitation of 50 nA up to 5 μA were applied to add on the dc current sweep from a Keithley 2400 with a bias resistor. A sum of current was then filtered and amplified using a bandpass pre-amplifier (figure S9).

TEM specimens were prepared by transferring carbon grid onto freshly exfoliated WTe_2 flakes on a SiO_2 wafer. A droplet of iso-propanol was applied onto the grid and let dry in air before peeling off the TEM grid. TEM observation was carried out using an FEI Tecnai-F20 system. The same few-layered WTe_2 flake (before and after degradation) was then observed under a 200 keV electron beam.

Acknowledgments

This work is supported by the National Natural Science Foundation of China with Grant 51522104 and 11504385. D M Sun thanks the National Natural Science Foundation of China with grant 51272256, 61422406, and 61574143. D Li acknowledges the National Natural Science Foundation of China with grant 51371175. Z D Zhang acknowledges supports from the National Natural Science Foundation of China with grant 51331006 and the Chinese Academy of Science under the project KJZD-EW-M05-3. V Bouchiat acknowledges support from the EU FP7 Graphene Flagship (project no. 604391), and the 2DTRANSFORMERS project under OH RISQUE program (ANR-14-OHRI-0004) of Agence Nationale de la Recherche (ANR).

References

[1] Ali M N *et al* 2014 Large, non-saturating magnetoresistance in WTe_2 *Nature* **514** 205
[2] Lee C-H, Silva E C, Calderin L, Nguyen M A T, Hollander M J, Bersch B, Mallouk T E and Robinson J A 2015 Tungsten ditelluride: a layered semimetal *Sci. Rep.* **5** 10013
[3] Kang D *et al* 2015 Superconductivity emerging from a suppressed large magnetoresistant state in tungsten ditelluride *Nat. Commun.* **6** 7804
[4] Soluyanov A A, Gresch D, Wang Z, Wu Q, Troyer M, Dai X and Bernevig B A 2015 Type-II Wyel semimetals *Nature* **527** 495–8
[5] Chang T-R *et al* 2016 Prediction of an arc-tunable Weyl Fermion metallic state in $Mo_xW_{1-x}Te_2$ *Nat. Commun.* **7** 10639
[6] Zhang K, Bao C, Gu Q, Ren X, Zhang H, Deng K, Wu Y, Li Y, Feng J and Zhou S 2016 Raman signatures of inversion symmetry breaking and structural phase transition in type-II Weyl semimetal $MoTe_2$ arXiv:1606.05071
[7] Deng K *et al* 2016 Experimental observation of topological Fermi arcs in type-II Weyl semimetal $MoTe_2$ *Nat. Phys.* **12** 1105
[8] Murzin S S, Dorozhkin S I, Landwehr G and Gossard A C 1998 Effect of hole-hole scattering on the conductivity of the two-component 2d hole gas in Gg/As/(AlGa)As heterostructures *J. Exp. Theor. Phys. Lett.* **67** 113
[9] Zhao Y F *et al* 2015 Anisotropic magnetotransport and exotic longitudinal linear magnetoresistance in WTe_2 crystals *Phys. Rev.* B **92** 041104(R)
[10] Wu Y, Jo N H, Mou D, Huang L, Bud'ko S L, Canfield P C and Kaminski A 2016 Observation of fermi arcs in type-ii Weyl semimetal candidate WTe_2 *Phys. Rev.* B **94** 121113(R)
[11] Wang C *et al* 2016 Spectroscopic evidence of type II Weyl semimetal state in WTe_2 arXiv:1604.04218

[12] Bruno F Y *et al* 2016 Surface states and bulk electronic structure in the candidate type-II Weyl semimetal WTe_2 *Phys. Rev.* B **94** 121112(R)
[13] Das P K *et al* 2016 Layer-dependent quantum cooperation of electron and hole states in the anomalous semimetal WTe_2 *Nat. Commun.* **7** 10847
[14] Ye F, Lee J, Hu J, Mao Z, Wei J and Feng P X-L 2016 Environmental instability and degradation of single- and few-layer WTe_2 nanosheets in ambient conditions *Small* **12** 5802
[15] Gao J, Li B, Tan J, Chow P, Lu T-M and Koratkar N 2016 Aging of transition metal dichalcogenide monolayers *ACS Nano* **10** 2628
[16] Mleczko M J, Xu R L, Okabe K, Kuo H-H, Fisher I R, Wong H-S P, Nishi Y and Pop E 2016 High current density and low thermal conductivity of atomically thin semimetallic WTe_2 *ACS Nano* **10** 7507
[17] Kim Y, Jhon Y I, Park J, Kim J H, Lee S and Jhon Y M 2016 Anomalous Raman scattering and lattice dynamics in mono- and few-layer WTe_2 *Nanoscale* **8** 2309
[18] Wang L, Gutiérrez-Lezama I, Barreteau C, Ubrig N, Giannini E and Morpurgo A F 2015 Tuning magnetotransport in a compensated semital at the atomic scale *Nat. Commun.* **6** 8892
[19] Woods J M, Shen J, Kumaravadivel P, Pang Y, Xie Y, Pan G A, Li M, Altman E I, Lu L and Cha J J 2016 Suppression of magnetoresistance in thin WTe_2 fakes by surface oxidation arXiv:1606.05756
[20] Wang Y, Wang K, Reutt-Robey J, Paglione J and Fuhrer M S 2016 Breakdown of compensation and persistence of nonsaturating magnetoresistance in gated WTe_2 thin flakes *Phys. Rev.* B **93** 121108(R)
[21] Jiang Y C, Gao J and Wang L 2016 Raman fingerprint for semi-metal WTe_2 evolving from bulk to monolayer *Sci. Rep.* **6** 19624
[22] Jana M K, Singh A, Late D J, Rajamathi C, Biswas K, Felser C, Waghmare U V and Rao C N R 2015 A combined experimental and theoretical study of the electronic and vibrational properties of bulk and few-layer Td-WTe_2 *J. Phys.: Condens. Matter* **27** 285401
[23] Lee J, Ye F, Wang Z H, Yang R, Hu J, Mao Z Q, Wei J and Feng P X-L 2016 Single- and few-layer WTe_2 and their suspended nanostructures: Raman signatures and nanomechanical resonances *Nanoscale* **8** 7854
[24] Wang L, Gutiérrez-Lezama I, Barreteau C, Ki D-K, Giannini E and Morpurgo A F 2016 Long-range field-effect from gate tuning of non-local conductivity *Phys. Rev. Lett.* **117** 176601
[25] Jager H, Haviland D B, Goldman A M and Orr B G 1986 Threshold for superconductivity in ultras thin amorphous gallium films *Phys. Rev.* B **34** 4920
[26] Kim B, Kwon D, Yajima T, Bell C, Kim B G, Hikita Y and Hwang H Y 2011 Reentrant insulating state in ultrathin manganite films *Appl. Phys. Lett.* **99** 092513
[27] Johnson H G, Bennett S P, Barua R, Lewis L H and Heiman D 2010 Universal properties of linear magnetoresistance in strongly disordered mnas-gaas composite semiconductors *Phys. Rev.* B **82** 085202
[28] Abrikosov A A 2000 Quantum linear magnetoresistance *Europhys. Lett.* **49** 789
[29] Hu J S and Rosenbaum T F 2008 Classical and quantum routes to linear magnetoresistance *Nat. Mater.* **7** 697
[30] Wang Z H, Yang L, Li X J, Zhao X T, Wang H L, Zhang Z D and Gao X P A 2014 Granularity controlled non-saturating linear magneto-resistance in topological insulator Bi_2Te_3 films *Nano Lett.* **14** 6510
[31] Wang Z H, Yang L, Zhao X T, Zhang Z D and Gao X P A 2015 Linear magneto-resistance versus weak antilocalization effects in Bi_2Te_3 films *Nano Res.* **8** 2963
[32] Larkin A I, Hikami S and Nagaoka Y 1980 Spin-orbit interaction and magnetoresistance in the two dimensional random system *Prog. Theor. Phys.* **63** 707
[33] Takagaki Y, Jenichen B, Jahn U, Ramsteiner M and Friedland K-J 2012 Weak antilocalization and electron–electron interaction effects in Cu-doped Bi_2Se_3 films *Phys. Rev.* B **85** 115314
[34] McCann E, Kechedzhi K, Fal'ko V I, Suzuura H, Ando T and Altshuler B L 2006 Weak-localization magnetoresistance and valley symmetry in graphene *Phys. Rev. Lett.* **97** 146805
[35] Zhao B, Cheng P, Pan H, Zhang S, Wang B, Wang G, Xiu F and Song F 2016 Weak antilocalization in Cd_3As_2 thin films *Sci. Rep.* **6** 22377
[36] Naylor C H *et al* 2016 Monolayer single-crystal 1T-$MoTe_2$ grown by chemical vapor deposition exhibits weak antilocalization effect *Nano Lett.* **16** 4297
[37] Zheng F *et al* 2016 On the quantum spin Hall gap of monolayer 1T-WTe_2 *Adv. Mater.* **28** 4845
[38] Li L K *et al* 2016 Quantum Hall effect in black phosphorus two-dimensional electron system *Nat. Nanotechnol.* **11** 593
[39] Cao Y *et al* 2015 Quality heterostructures from two dimensional crystals unstable in air by their assembly in inert atmosphere *Nano Lett.* **15** 4914